Optics Letters

Femtosecond laser inscribed helical sapphire fiber Bragg gratings

Qi Guo,[1] Shanren Liu,[1] Xuepeng Pan,[1] Bo Wang,[1] Zhennan Tian,[1] Chao Chen,[2] Qidai Chen,[1] Yongsen Yu,[1,*] and Hongbo Sun[1,3]

[1]State Key Laboratory of Integrated Optoelectronics, College of Electronic Science and Engineering, Jilin University, 2699 Qianjin Street, Changchun 130012, China
[2]Changchun Institute of Optics, Fine Mechanics and Physics, Chinese Academy of Sciences, Changchun 130033, China
[3]State Key Laboratory of Precision Measurement Technology and Instruments, Department of Precision Instrument, Tsing-Hua University, Haidian, Beijing 100084, China
*Corresponding author: yuys@jlu.edu.cn

Received 3 August 2021; revised 1 September 2021; accepted 7 September 2021; posted 8 September 2021 (Doc. ID 439373); published 27 September 2021

This Letter reports a novel helical sapphire fiber Bragg grating (HSFBG) in a single crystal sapphire fiber with diameter of 60 μm fabricated by a 515 nm femtosecond laser. Due to the large refractive index modulation region and high structural symmetry of the HSFBGs, high-reflectivity and high-quality spectra can be prepared and additionally have good bending resistance. The spectral properties of HSFBGs with different helical diameters are studied. When the helical diameter is 30 μm, the reflectivity of HSFBG is 40%, the full width at half-maximum is 1.56 nm, and the signal-to-noise ratio is 16 dB. For the HSFBG bending test, the minimum bending radius is 5 mm, which can still maintain relatively good spectral quality. In addition, the HSFBG array with different periods has been successfully cascaded in a sapphire fiber. The experimental results of the HSFBG high-temperature test show that this HSFBG can work reliably at 1600°C, and the temperature sensitivity in the high-temperature range can reach 35.55 pm/°C. This HSFBG can be used in high-temperature and harsh environments, such as metal smelting and aeroengine structural health monitoring.

https://doi.org/10.1364/OL.439373

The femtosecond laser has the advantages of ultra-short pulse width and ultra-high peak power [1], which can be used for laser additive and subtractive manufacturing of different materials to realize the preparation of three-dimensional structures and devices [2–6]. When the peak power of the laser exceeds the nonlinear absorption threshold of material, a multiphoton absorption nonlinear effect will occur, which will induce permanent refractive index change inside transparent material [7,8]. With the gradual maturity of femtosecond laser processing technology and the improvement of fiber grating preparation level, different types of gratings can be fabricated in quartz fiber [9], mid-infrared fiber [10], and crystal fiber [11]. However, due to the limitation of quartz softening temperature, quartz fibers are difficult to continue to be used above 1200°C [12]. In recent years, the appearance of crystal fiber provides a novel idea for the field of fiber high-temperature sensing. Taking a sapphire fiber as an example, it has the advantages of high melting point (2053°C), wide transmission spectrum, and chemical corrosion resistance. Through femtosecond laser processing technology, the permanent refractive index modulation can be realized inside the sapphire fiber, so as to prepare fiber high-temperature sensors.

The main methods for preparing sapphire fiber Bragg gratings (SFBGs) are the phase mask method [13], femtosecond laser point by point (PbP) method [14], and femtosecond laser line by line (LbL) scanning method [15]. In 2004, Grobnic *et al.* prepared the SFBGs for the first time, to the best of our knowledge, in a sapphire fiber with a diameter of 150 μm by using an 800 nm femtosecond laser combined with the phase mask method [13]. In order to solve the limitation of the fixed pitch of a phase mask, Elsmann *et al.* proposed a Talbot interferometer system in 2013 and prepared an SFBG array with different periods [16]. Compared with the phase mask method, the femtosecond laser PbP method is more flexible. In 2017, Yang *et al.* successfully fabricated SFBGs with reflectivity of 0.6% in a 125 μm diameter sapphire fiber by the femtosecond laser PbP method [14]. In order to solve the problem of small refractive index modulation region and low reflectivity when preparing SFBGs by the PbP method, Xu *et al.* successfully prepared the SFBGs with reflectivity of 6.3% in a 60 μm diameter sapphire fiber using the LbL scanning method in 2018 [15]. In order to further increase the refractive index modulation region and improve the reflectivity, they proposed the LbL scanning double-layer method in 2019 and successfully prepared SFBGs with reflectivity of 34.1% [17].

In this Letter, we report a novel three-dimensional structure and method for preparing SFBGs. This kind of helical SFBGs (HSFBGs) has a large refractive index modulation region and good structural symmetry. We have studied the reflection spectrum characteristics of HSFBGs with different helical diameters and tested the high-temperature stability of HSFBGs cyclically. In addition, the HSFBG array with different periods is successfully cascaded in a sapphire fiber.

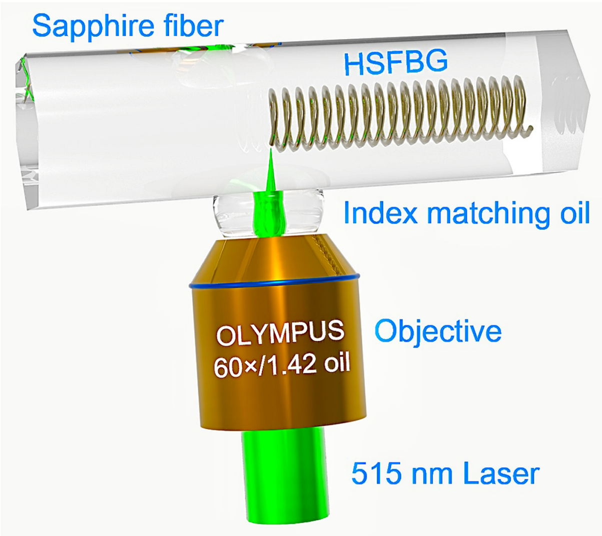

Fig. 1. Experimental setup of HSFBGs inscribed in a 60 μm sapphire fiber.

Figure 1 is the experimental setup of HSFBGs prepared in sapphire fiber (MicroMaterials Inc.) with a diameter of 60 μm. The femtosecond laser (light conversion) used has a working wavelength of 1030 nm, a pulse width of 290 fs, and an adjustable repetition frequency of up to 200 kHz. The frequency doubling crystal ($\beta - BaB_2O_4$) is used to convert a 1030 nm laser to a 515 nm laser [18]. The laser with the shorter wavelength is conducive to the realization of finer processing. In the experiment, the single-pulse energy and laser repetition frequency used are 90 nJ and 1 kHz, respectively. The 515 nm laser is focused into the sapphire fiber placed on the five-dimensional processing platform (Aerotech ABL10050L) through an oil immersion objective lens (Olympus 60 × /1.42). By setting parameters such as helical diameter and helical pitch in the software, the three axes XYZ of the processing platform will perform combined helical motion under program control, and the helical trajectory will be scanned inside the sapphire fiber by the focused femtosecond laser. The moving speed of the platform along the sapphire fiber axis is 0.004 mm/s.

The fiber Bragg grating (FBG) phase matching condition is $m\lambda_B = 2n_{\text{eff}}\Lambda$, where m is the grating order, λ_B is the resonant wavelength, n_{eff} is the effective refractive index, and Λ is the grating period. The helical diameter of the prepared HSFBG is 30 μm, the grating period is 1.332 μm, the grating order is $m = 3$, and the grating length is 4 mm. The refractive index of sapphire is 1.746 (at 1550 nm), and the center wavelength of the prepared third-order HSFBG is about 1550 nm.

Figure 2 shows the micrograph comparison of helical gratings with different periods and different helical diameters. Figures 2(a) and 2(b) are micrograph comparisons of HSFBGs with a period of 1.332 μm and helical diameters of 15 μm and 30 μm, respectively. In order to further see the processing effect of helical gratings clearly, the gratings with larger helical pitch are prepared. Figures 2(c) and 2(d) are micrograph comparison of HSFBGs with a period of 6.66 μm and helical diameters of 15 μm and 30 μm, respectively. The uniform helical trajectory left by laser scanning can be clearly seen from Fig. 2. Figure 2(c) can clearly show the three-dimensional structure of the helical

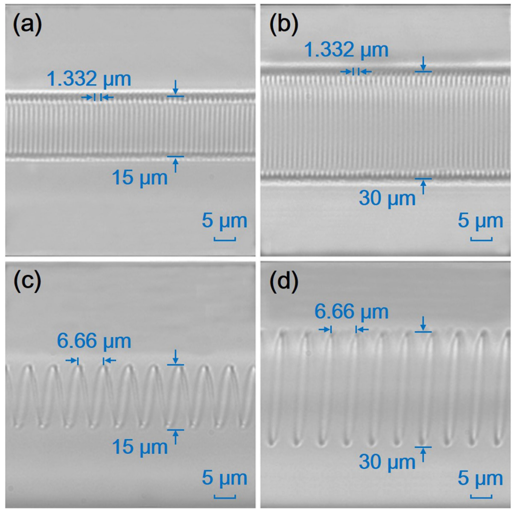

Fig. 2. (a) and (b) are micrographs of HSFBGs with the period of 1.332 μm and the helical diameters of 15 μm and 30 μm, respectively. (c) and (d) are micrographs of HSFBGs with the period of 6.66 μm and the helical diameters of 15 μm and 30 μm, respectively.

grating. The different thickness and sharpness of the trajectory are caused by the different focusing depth of the microscope.

Figure 3 shows the spectral comparison of HSFBGs with different helical diameters of 15, 20, 25, 30, and 35 μm, which are tested by multimode fiber coupling. The illustration is a partial enlarged view in the range of 20 nm. It can be seen that the reflectivity of HSFBGs prepared with different helical diameters is similar. This is because the reflectivity is determined not only by the size of the refractive index modulation region, but also by the area of the effective coupling region between the refractive index modulation region and the mode field region. Increasing the helical diameter in a certain range will increase the overlapping region of the refractive index modulation region and mode field and increase the reflectivity. When the helical diameter continues to increase, because the intensity of the mode field close to the edge of the sapphire fiber decreases, even if the refractive index modulation region increases, the effective overlapping region with the mode field decreases, and the reflectivity also decreases. In this experiment, the helical diameter of the tested HSFBG is 30 μm.

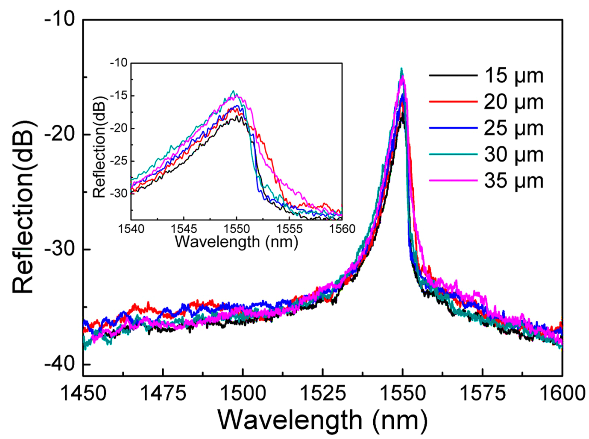

Fig. 3. Spectral comparison of HSFBGs with different helical diameters of 15 μm, 20 μm, 25 μm, 30 μm, and 35 μm. The illustration is a partial enlarged view in the range of 20 nm.

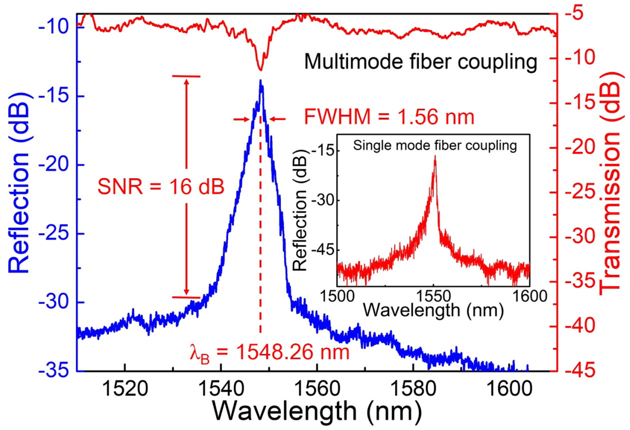

Fig. 4. HSFBG reflection and transmission spectra obtained by multimode fiber coupling. The illustration is the HSFBG reflection spectrum obtained by single-mode fiber coupling.

The sapphire fiber and quartz multimode fiber (62.5/125 μm) are spliced by a fusion splicer (FSU975). The discharge current is set to 10 mA, and the discharge time is 1.5 s. Figure 4 shows the reflection and transmission spectra of a third-order HSFBG with a helical diameter of 30 μm and grating period of 1.332 μm. The center wavelength of the HSFBG is 1548.26 nm, the full width at half-maximum (FWHM) is 1.56 nm, and the signal-to-noise ratio (SNR) is 16 dB. The inset in Fig. 4 shows the spectral effect measured by the single-mode fiber coupler. It can be seen that there are many burrs in the reflection spectrum coupled by the single-mode fiber, which is caused by the high multimode of the sapphire fiber. Different spatial modes of the multimode fiber have a different mode effective refractive index, which corresponds to different Bragg wavelengths when coupled with the single-mode fiber [19]. In addition, some high-order modes will be filtered out through single-mode fiber coupling, the reflection peak will be narrowed, and the FWHM will be reduced. However, because the mode field diameter of the single-mode fiber does not match that of the sapphire fiber, the mode is easily unstable when the external disturbance occurs. The multimode fiber has larger mode field diameter, and the reflection spectrum can be coupled as a whole envelope through the multimode fiber, so that the spectrum is more stable, and the mode jump does not occur easily.

With the increase of sapphire fiber length and the existence of surface defects, more high-order modes will be excited. When the sapphire fiber is bent or disturbed, the mode energy distribution transmitted in the fiber also fluctuates, showing a random distribution in a certain range. This will change the coupling efficiency between the refractive index modulation region and the mode field region, make the spectrum unstable, and split the reflection peak or change the reflectivity.

The helical gratings have good structural symmetry and large refractive index modulation region. When there is external disturbance and the mode field intensity is redistributed in a certain range, it can still maintain a relatively stable coupling efficiency. This can reduce the influence of sapphire fiber bending or disturbance and fiber surface defects on the spectral quality. The bending resistance and spectral stability of HSFBGs can be tested by bending the sapphire fiber. Figure 5(a) shows the process of bending the sapphire fiber at different bending radii,

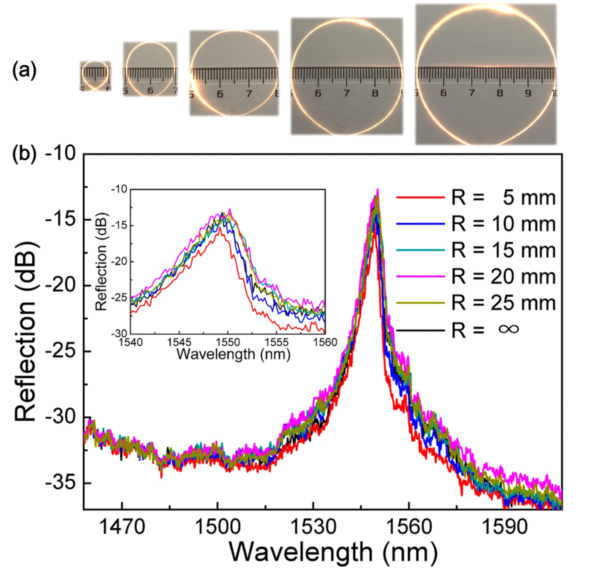

Fig. 5. (a) Bending test process of HSFBG. (b) Spectral response of HSFBG at different bending radii. The illustration is a partial enlarged view in the range of 20 nm.

and Fig. 5(b) shows the spectral response of HSFBGs. The illustration shows the central part of the spectrum in the range of 20 nm in order to more clearly show the filtering effect of high-order modes during sapphire fiber bending.

When the bending radius is gradually reduced to 10 mm, the reflectivity basically remains unchanged. When the sapphire fiber is bent continuously and the bending radius is 5 mm, the reflectivity decreases slightly, and the spectrum becomes smoother than that without bending. This is mainly because the bending process will filter out some high-order modes in the sapphire fiber, which will smooth the spectrum and reduce the FWHM accordingly. The bending test shows that HSFBGs have good spectral stability. In addition, the HSFBG array with different wavelengths of 1520.05 nm, 1550.39 nm, and 1580.42 nm are fabricated in the sapphire fiber with the length of 30 cm. The distribution of gratings is shown in Fig. 6(a). The light of the broadband light source is from port A to port B. Figure 6(b) is the measured reflection spectrum.

The customized high-temperature furnace with maximum temperature of 1600°C is used to test the HSFBGs. It can heat from room temperature to 1600°C and hold for 3 h for thermal annealing treatment to eliminate internal stress and unstable structures caused by laser processing. The temperature response of HSFBG is retested after annealing. The heating process is from room temperature to 1600°C with temperature intervals of 100°C. Each temperature point is maintained for 30 min to ensure the stability of the temperature. The cooling process is from 1600°C to room temperature, which is the opposite of the heating process. Figure 7 shows the relationship between temperature and wavelength through quadratic fitting, which can obtain a good fitting effect. This nonlinear thermal response can be given by the quadratic fitting function: $\lambda = A + B \cdot T + C \cdot T^2$, where the values of A, B, and C are 1548.01361 nm, 0.02127 nm/°C, and 5.40458×10^{-6} nm/°C^2, respectively. The relationship between temperature and wavelength in different temperature ranges is linearly fitted. The temperature sensitivity is 24.42 pm/°C (0–500°C),

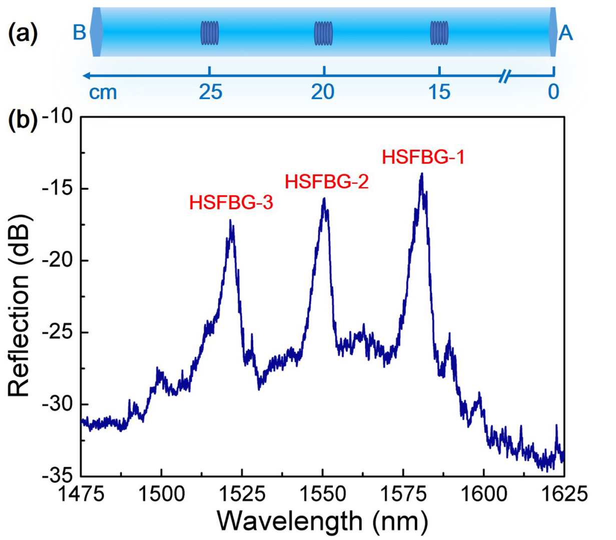

Fig. 6. (a) Schematic diagram of HSFBG array with different periods inscribed in different positions of the sapphire fiber. (b) Reflection spectrum of HSFBG array measured from end A.

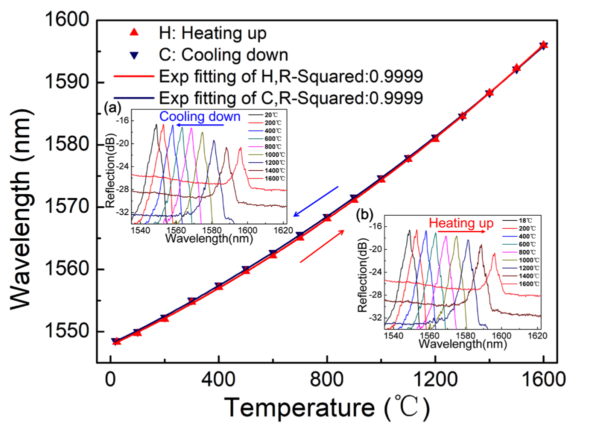

Fig. 7. Bragg wavelength of HSFBGs varies with temperature. The illustrations show the change of the HSFBG reflection spectrum with temperature during (a) cooling process and (b) heating process.

29.26 pm/°C (500–1000°C), and 35.55 pm/°C (1000-1600°C), respectively. Figures 7(a) and 7(b) are the curves of wavelength drift with temperature during the cooling and heating processes, respectively. It can be seen from the heating and cooling process that the HSFBGs have good temperature stability and repeatability.

In conclusion, we fabricate the HSFBGs in a 60 μm diameter sapphire fiber by 515 nm femtosecond laser direct writing system and test their performance parameters. A novel three-dimensional structure and method for preparing SFBGs with high reflectivity and high spectral quality has been proposed and verified. The spectra of HSFBGs with different helical diameters are compared. The HSFBG with a helical diameter of 30 μm has been successfully prepared, with reflectivity of 40%, FWHM of 1.56 nm, and SNR of 16 dB. In addition, the HSFBG array with different wavelengths is successfully cascaded in a sapphire fiber. The high-reflectivity and high-quality spectra can be prepared due to the large refractive index modulation region and high structural symmetry of the HSFBGs. The high-temperature test shows that the HSFBGs can work stably at 1600°C, and the temperature sensitivity in the high-temperature range is 35.55 pm/°C, which has good temperature repeatability and stability. This kind of HSFBG has important application value in high-temperature and harsh environments, such as metal smelting and aerospace.

Funding. National Natural Science Foundation of China (62090064, 91860140, 61874119, 62131018); Science and Technology Development Project of Jilin Province (20180201014GX).

Disclosures. The authors declare no conflicts of interest.

Data Availability. Data underlying the results presented in this Letter are not publicly available at this time but may be obtained from the authors upon reasonable request.

REFERENCES

1. Y. Liao, J. Xu, H. Y. Sun, J. Song, X. S. Wang, and Y. Cheng, Appl. Surf. Sci. **254**, 7018 (2008).
2. Z. Z. Li, L. Wang, H. Fan, Y. H. Yu, H. B. Sun, S. Juodkazis, and Q. D. Chen, Light Sci. Appl. **9**, 41 (2020).
3. C. Xie, R. Meyer, L. Froehly, R. Giust, and F. Courvoisier, Light Sci. Appl. **10**, 126 (2021).
4. L. Wang, Q. D. Chen, X. W. Cao, R. Buividas, X. W. Wang, S. Juodkazis, and H. B. Sun, Light Sci. Appl. **6**, e17112 (2017).
5. Z. C. Ma, Y. L. Zhang, B. Han, X. Y. Hu, C. H. Li, Q. D. Chen, and H. B. Sun, Nat. Commun. **11**, 4536 (2020).
6. X. Li and Y. Guan, Nanotechnol. Precis. Eng. **3**, 105 (2020).
7. J. Thomas, C. Voigtlander, R. G. Becker, D. Richter, A. Tunnermann, and S. Nolte, Laser Photon. Rev. **6**, 709 (2012).
8. Y. Zhao, Y. Yang, and H.-B. Sun, PhotoniX **2**, 3 (2021).
9. S. J. Mihailov, C. W. Smelser, D. Grobnic, R. B. Walker, P. Lu, H. M. Ding, and J. Unruh, J. Lightwave Technol. **22**, 94 (2004).
10. M. Bernier, D. Faucher, R. Vallee, A. Saliminia, G. Androz, Y. Sheng, and S. L. Chin, Opt. Lett. **32**, 454 (2007).
11. H. Chen, M. Buric, P. R. Ohodnicki, J. Nakano, B. Liu, and B. T. Chorpening, Appl. Phys. Rev. **5**, 011102 (2018).
12. S. J. Mihailov, Sensors **12**, 1898 (2012).
13. D. Grobnic, S. J. Mihailov, C. W. Smelser, and H. M. Ding, IEEE Photon. Technol. Lett. **16**, 2505 (2004).
14. S. Yang, D. Hu, and A. B. Wang, Opt. Lett. **42**, 4219 (2017).
15. X. Z. Xu, J. He, C. R. Liao, K. M. Yang, K. K. Gu, C. Li, Y. F. Zhang, Z. B. Ouyang, and Y. P. Wang, Opt. Lett. **43**, 4562 (2018).
16. T. Elsmann, T. Habisreuther, A. Graf, M. Rothhardt, and H. Bartelt, Opt. Express **21**, 4591 (2013).
17. X. Z. Xu, J. He, C. R. Liao, and P. P. Wang, Opt. Lett. **44**, 4211 (2019).
18. R. Klas, A. Kirsche, M. Gebhardt, J. Buldt, H. Stark, S. Hädrich, J. Rothhardt, and J. Limpert, PhotoniX **2**, 4 (2021).
19. Y.-G. Nan, D. Kinet, K. Chah, I. Chapalo, C. Caucheteur, and P. Mégret, Opt. Express **29**, 25824 (2021).